MedChemComm

RESEARCH ARTICLE

View Article Online
View Journal | View Issue

Cite this: *Med. Chem. Commun.*, 2018, **9**, 503

Exploring eukaryotic *versus* prokaryotic ribosomal RNA recognition with aminoglycoside derivatives†

Narayana Murthy Sabbavarapu,[a] Tomasz Pieńko,[bc] Bat-Hen Zalman,[a] Joanna Trylska *[b] and Timor Baasov *[a]

Received 1st January 2018,
Accepted 31st January 2018

DOI: 10.1039/c8md00001h

rsc.li/medchemcomm

New derivatives of aminoglycosides containing 6′-carboxylic acid or 6′-amide on their ring I were designed, synthesized and their ability to readthrough nonsense mutations was examined *in vitro*, along with the protein translation inhibition in prokaryotic and eukaryotic systems. The observed structure–activity relationships, along with the comparative molecular dynamics simulations within the eukaryotic rRNA decoding site, showed high sensitivity of 6′-position to substitution, indicating that the rational design of potent stop-codon read-through inducers requires consideration of not only the structure and energetics of the drug–RNA interaction but also the dynamics associated with that interaction.

Introduction

Aminoglycosides (AGs) are well known antibiotics that specifically bind to the decoding-site RNA within the small ribosomal subunit, and thereby interfere with translation fidelity, leading to bacterial cell death.[1] In the last several years, it was shown that some AG antibiotics can also impact the eukaryotic ribosome and promote read-through of premature termination codons (PTCs) in mRNA. This unique phenomenon of AGs, also termed "PTC suppression" or "translational readthrough", has been demonstrated in several *in vitro* and *in vivo* experiments including clinical trials.[2] AGs are therefore considered as potential therapeutics for PTC underlined genetic disorders. However, the lack of potency of standard AGs and their recognized nephrotoxicity and ototoxicity at high doses encouraged further research towards the development of new derivatives.[3]

During last several years, we systematically developed a series of lead compounds,[4] which was found to improve readthrough activity and reduce toxicity as demonstrated in various models of a variety of different diseases underlying by PTC mutations.[5,6] Because of the lack of detailed molecular data on the interaction of AGs within their eukaryotic target site, all those lead structures were developed based on the reported structural data of conventional AGs within the prokaryotic target site, and their subsequent biochemical and toxicity data. Recent structural and mechanistic insights on the interaction of AGs with eukaryotic ribosome, provided reasonable basis for structure-based rational design of novel read-through inducers.[6]

The crystal structure of the AG geneticin (G418) bound to 80S yeast ribosome,[7] along with the structures of G418 (ref. 8) and paromomycin[9] bound to their putative binding site of *Leishmania* ribosomes, are among recently reported structures deciphering the interaction of AGs with the eukaryotic ribosomal target. Based on these structural data, we very recently reported on the design, synthesis and evaluation of the new lead structure **2** that differs from its parent structure **1** by the presence of an additional hydroxyl on the side-chain of the glucosamine ring (ring I) (compounds **1** and **2** are also named NB124 and NB157, respectively, Fig. 1).[10] Preliminary modeling study suggested that the extension of the side-chain methyl group in compound **1** so as to generate 6′,7′-diol in **2**, could allow additional H-bond interaction and subsequently increased specificity toward eukaryotic ribosome. Indeed, compound **2** showed substantially enhanced specificity to the eukaryotic cytoplasmic ribosome and induced higher PTC read-through in comparison to that of **1**.[10] Encouraged, we reasoned that converting the primary 6′-OH group in the previously reported **4** and **5** (ref. 4) to the corresponding 6′-carboxylic acid or 6′-amide would improve the binding of new derivatives into the eukaryotic ribosome, and subsequently increase the PTC read-through activity. To test this hypothesis, herein we report on the design, synthesis and evaluation of a series of pseudo-disaccharides (**6** and **7**)

[a] *The Edith and Joseph Fischer Enzyme Inhibitors Laboratory, Schulich Faculty of Chemistry, Technion – Israel Institute of Technology, Haifa 32000, Israel. E-mail: chtimor@tx.technion.ac.il; Tel: +972 4 829 2590*
[b] *Centre of New Technologies, University of Warsaw, Banacha 2c, 02-097 Warsaw, Poland. E-mail: joanna@cent.uw.edu.pl; Tel: +48 22 554 3683*
[c] *Department of Drug Chemistry, Faculty of Pharmacy with the Laboratory Medicine Division, Medical University of Warsaw, Banacha 1a, 02-097 Warsaw, Poland*

† Electronic supplementary information (ESI) available: Simulation methods, biochemical assays, synthetic procedures, and copies of NMR spectra (PDF). See DOI: 10.1039/c8md00001h

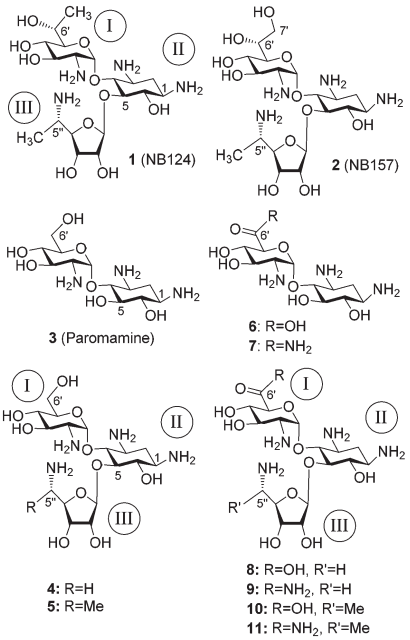

Fig. 1 Chemical structures of synthetic AGs that were investigated in this study.

and pseudo-trisaccharides (**8–11**), exhibiting either carboxylic acid or amide function at 6′-position of the glucosamine ring (ring I) (Fig. 1).

Results and discussion

In selecting the 6′-acid and 6′-amide in **6–11**, we have taken into consideration the following points. Firstly, from the available data on AGs as readthrough inducers, it has been well documented that AGs containing a 6′-OH on their ring I (such as G-418 and paromomycin) are more effective than those with the amine functionality at the same position.[6,11] These observations are usually rationalized by one of the main differences between their putative binding sites in eukaryotic *vs.* prokaryotic ribosomes: the 1408 position (*E. coli* numbering, A1408 in bacteria and G1408 in eukaryotes).[12] It has been suggested that while both 6′-OH and 6′-NH_2 can form H-bond interactions with A1408 in bacterial ribosomes, the 6′-NH_2 derivatives are prevented from such interactions with G1408 in eukaryotic ribosomes due to the electrostatic repulsion between the positively charged nitrogen atom of the guanine residue and the 6′-ammonium of AGs.[13] Second, the observed differential selectivity in regards to the substitution at the 6′ position, is further supported by the data showing that 6′-NH_2 AGs are less effective against the growth of eukaryotic parasite *Leishmania*[8] and against AG resistant bacterial strains containing A1408G mutation.[13] Finally, we have demonstrated that the increased specificity toward eukaryotic cytoplasmic ribosome correlates with increased PTC suppression activity.[4] These observations, along with our own modeling studies, suggested that a planar 6′-carboxylate on ring I might serve as an acceptor of hydrogen bonds from the Watson–Crick site of the G1408 N1 and N2 amino groups, thereby significantly improve the affinity towards the eukaryotic *versus* the prokaryotic ribosome (Fig. 2). Similarly, the planar 6′-amide enhances the efficacy of the ligands to improve the PTC suppression activity. We expected that the proposed structural manipulations, 6′-acid and 6′-amide in **6–11**, would preserve all the existing crucial interactions of the parent AG (with 6′-OH) to the ribosomal RNA, while the additional interactions generated due to added 6′-acid and/or 6′-amide would increase binding affinity and subsequent PTC read-through activity of the resulting structure.

The synthesis of **6** and **7** are illustrated in Scheme 1. The known[14] compound **12**, was selectively protected at the primary hydroxyl, followed by protection of all the secondary hydroxyls with benzoate esters to afford the completely protected **13**. Treatment with HF/Py gave the corresponding 6′-alcohol, which was subsequently oxidized using TEMPO/BIAB[15] to afford the acid **14**.

Base hydrolysis was followed by the Staudinger reaction to produce **6** with 6′-CO_2H functionality. The corresponding 6′-$CONH_2$ was synthesized from the intermediate acid **14** by following the procedure reported by Hermann and co-workers[16] with some modifications. To a precooled mixture of DMF and oxalyl chloride at −30 °C was added the intermediate 6′-acid **14** to generate the corresponding acid chloride. The reaction mixture was cooled to −78 °C and the ammonia gas was condensed into the vessel. *In situ* generated acid chloride reacted with ammonia to afford the amide **15**. Once again, base hydrolysis followed by the Staudinger reaction produced the fully deprotected target 6′-amide **7**. The assembly of the pseudo-trisaccharides **8–11** is illustrated in Scheme 2.

The intermediate 6′-silyl ether (Scheme 1) was subjected to a regioselective benzoylation (BzCl) to yield the corresponding C5 acceptor **16**. Glycosylation with the trichloroacetimidate donors **17** (ref. 4) and **18** (ref. 4) in the presence of catalytic $BF_3{\cdot}OEt_2$ afforded the protected pseudo-trisaccharides **19** and **20** exclusively as β-anomers in excellent

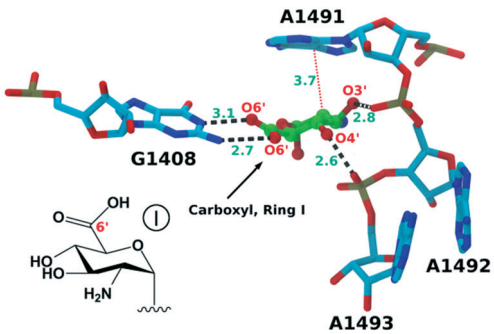

Fig. 2 Three-dimensional structure of ring I of compound **8** docked into the 80S ribosome from *S. cerevisiae* (PDB code 4U4O)[7] highlighting the interactions of only its ring I (green) into the decoding-site rRNA (*E. coli* numbering). Atom coloring: C – cyan, O – red, N – blue, P – brown. H-Bonds (dashed black lines) and C–H···π stacking (dotted red line) are shown. The inset shows chemical structure of ring I of **8**.

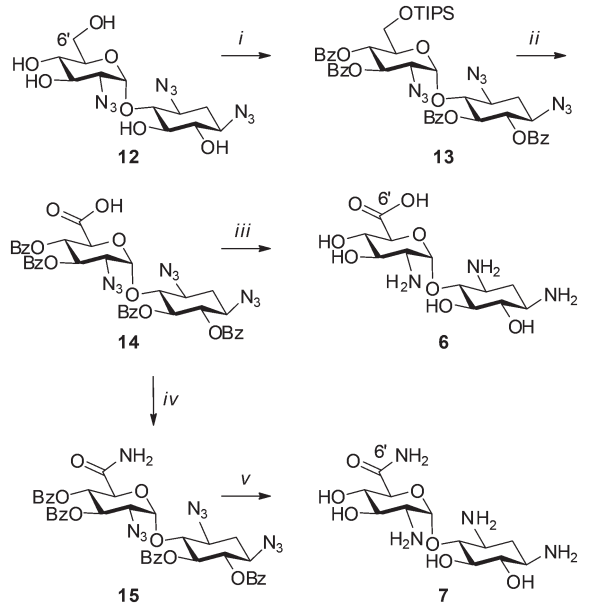

Scheme 1 Reagents and conditions: (i) (a) TIPSCl, DMF, 4-DMAP, 0–25 °C, 83%; (b) BzCl, 4-DMAP, Py, 80 °C, 80%; (ii) (a) HF/Py, Py, 0–4 °C, 82%; (b) TEMPO, BIAB, CH_2Cl_2:H_2O, 5 °C, 100%; (iii) (a) NaOMe, MeOH, 0–60 °C, 88%; (b) PMe_3, THF, NaOH (0.1 M), 67%; (iv) (a) oxalyl chloride $(COCl)_2$, DMF, CH_2Cl_2, −30–0 °C, then NH_3(gas), −78–0 °C, 62%; (v) NaOMe, MeOH, 0–60 °C, 77%; (b) PMe_3, THF, NaOH (0.1 M), 57%.

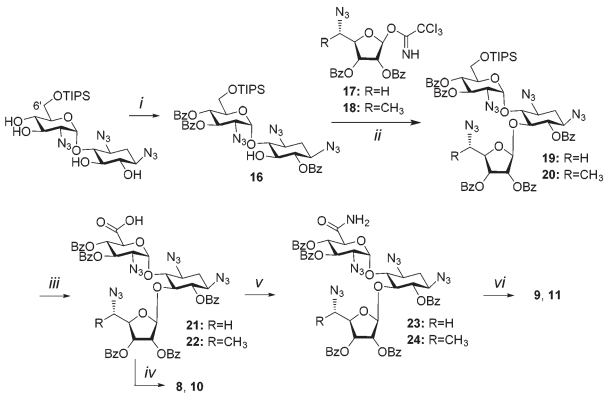

Scheme 2 Reagents and conditions: (i) BzCl, 4-DMAP, Py, −5 °C, 44%; (ii) BF_3–OEt_2, CH_2Cl_2, −30 °C; (iii) (a) HF/Py, Py, 0–4 °C; (b) TEMPO, BIAB, CH_2Cl_2:H_2O, 5 °C, 92% of **21**, 94% of **22**; (iv) (a) NaOMe, MeOH, 0–60 °C, 89% (R═H), ~100% (R═CH_3); (b) PMe_3, THF, NaOH (0.1 M), 58% of **8**, 72% of **10**; (v) oxalyl chloride $(COCl)_2$, DMF, CH_2Cl_2, −30–0 °C, then NH_3 (gas), −78–0 °C, 69% of **23**, 71% of **24**; (vi) (a) NaOMe, MeOH, ~100% (R═H), ~100% (R═CH_3); (b) PMe_3, THF, NaOH (0.1 M), 47% of **9**, 71% of **11**.

isolated yields. Treatment of the silyl ether products with HF/Py furnished the corresponding 6′-alcohols, which after oxidation provided the corresponding 6′-acids **21** and **22**. Hydrolysis of the benzoate esters was followed by the Staudinger reaction to afford the target 6′-acids, **8** and **10**. For the synthesis of the pseudo-trisaccharides with 6′-amide, the intermediate 6′-acids **21** and **22** were first converted to the corresponding 6′-amides **23** and **24**; two subsequent deprotection steps provided the target 6′-amides **9** and **11**. The structures of all new compounds were confirmed by a combination of various 1D and 2D NMR techniques, including 1D TOCSY, 2D COSY, 2D ^1H–^{13}C HMQC and HMBC, along with mass spectrometry.

Initially, we tested **6** and **7** for *in vitro* PTC suppression efficacy (Fig. 3A). The observed data show that oxidation of 6′-OH in **3** to yield the 6′-acid in **6**, is accompanied with a significant reduction in readthrough activity. This reduction in activity is even more significant in the 6′-amide **7**. The observed reduction in the PTC suppression activity of **6** and **7** was further supported by their significantly reduced inhibition of the eukaryotic protein translation process (Table 1). The measured half maximal inhibitory concentration values, IC_{50}^{Euk}, for **6** and **7** are 5.4-fold and 4.0-fold higher compared to that of **3**. When the same comparative translation inhibition tests were performed in the prokaryotic system, the negative impacts of both **6** and **7** *versus* that of **3** were more substantial. For example, the 6′-acid **6** is 293-fold poorer inhibitor than the paromamine **3** (IC_{50}^{Pro} = 0.01 mM and 2.93 mM, for **6** and **3**, respectively). The comparative PTC suppression and translation inhibition data with the pseudo-disaccharides **3**, **6** and **7** (Fig. 3 and Table 1) show that the conversion of 6′-OH to corresponding 6′-CO_2H or 6′-$CONH_2$ significantly reduces the compounds' ability to inhibit protein translation process and that this effect is much stronger in the prokaryotic than in the eukaryotic system. Importantly, our comparative data on the pseudo-disaccharides **3**, **6** and **7** in regards to the bacterial ribosome, are in agreement with that previously reported by Hermann and co-workers.[16] This group synthesized **6** and **7** and tested them for their impact only on the inhibition of prokaryotic protein synthesis. Both **6** and **7** were about 2-order of magnitude poorer inhibitors than the parent **3** (IC_{50}^{Pro} values of 3.9, 620 and >100 μM for

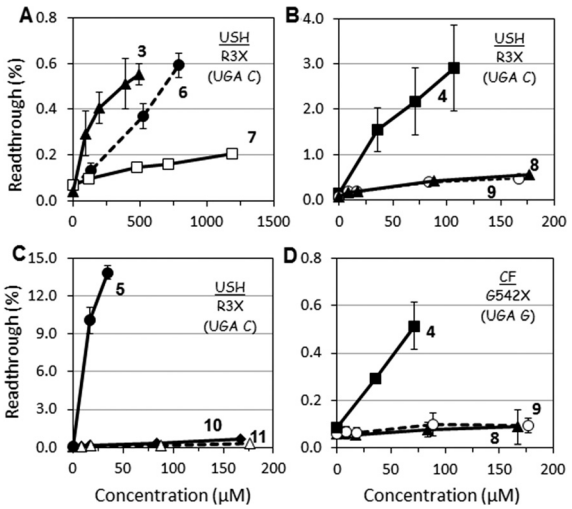

Fig. 3 Comparative *in vitro* stop codon suppression levels induced by pseudo-disaccharides (A) paromamine **3**, 6′-acid **6** and 6′-amide **7**, and by pseudo-trisaccharides (B and D) compounds **4**–**5**, **8**–**11** in two different nonsense constructs representing genetic diseases (shown in parenthesis): (A–C) R3X (USH1) and (D) G542X (CF). The assays were performed as previously described by us.[4] The results are averages of at least three independent experiments.

Table 1 Comparative translation inhibition and antibacterial activity tests[a]

	Translation inhibition[b]			Antibacterial activity MIC[c] (μg mL^{-1})	
Comp.	IC_{50}^{Euk} (mM)	IC_{50}^{Pro} (mM)	$\frac{IC_{50}^{Euk}}{IC_{50}^{Pro}}$	*E. coli* R477/100	*B. subtilis* ATCC6633
3	0.80 ± 0.08	0.01 ± 0.00	80	>192	>192
6	4.32 ± 0.69	2.93 ± 0.57	1.5	>192	>192
7	3.18 ± 0.42	2.41 ± 0.29	1.3	>192	>192
4	0.03 ± 0.00	0.0005 ± 0.0000	60	790	100
8	0.70 ± 0.07	1.30 ± 0.10	0.5	>192	>192
9	0.50 ± 0.04	0.42 ± 0.04	1.2	>192	>192
5	0.02 ± 0.00	0.002 ± 0.000	10	2659	83
10	0.60 ± 0.05	1.30 ± 0.08	0.5	>192	>192
11	0.52 ± 0.04	2.31 ± 0.32	0.2	>192	>192

[a] All tested compounds, in all biological tests, were in their sulfate salt forms and the concentrations reported refer to that of the free amine form of each AG. [b] Prokaryotic (IC_{50}^{Pro}) and eukaryotic (IC_{50}^{Euk}) translation inhibition values were quantified as previously described by us.[4] [c] The MIC values were determined by using the double-microdilution method.

3, **6** and **7**, respectively), indicating that the chemical function at the 6′-position of AGs is pivotal in bacterial target site recognition.

In fact, these previous data of **3**, **6** and **7** with the prokaryotic system was the main trigger for our current work. Thus, while our observed data with the prokaryotic system is similar to that of Hermann and co-workers, the scenario in the eukaryotic system is significantly different (Table 1). While the compound **3** is 80-fold more selective towards prokaryotic *versus* eukaryotic ribosome ($IC_{50}^{Euk}/IC_{50}^{Pro}$ = 80) this selectivity is dramatically reduced for the compounds **6** and **7**, $IC_{50}^{Euk}/IC_{50}^{Pro}$ values of 1.5 and 1.3, respectively. The observed differential selectivity of the pseudo-disaccharides **6** and **7** *versus* that of the parent **3** was very intriguing and we were interested to know whether this trend would be retained in the corresponding pseudo-trisaccharides.

To test this issue, the pseudo-trisaccharides with the 6′-acid, compounds **8** and **10**, and with the 6′-amide, compounds **9** and **11**, were separately evaluated against their parent structures **4** and **5**, respectively (Fig. 3). For the PTC suppression tests we used the nonsense reporter plasmids R3X for Usher syndrome (USH) and G542X for cystic fibrosis (CF). The observed data in Fig. 3 show that none of the pseudo-trisaccharides (**8–11**) exhibit superior activity to the corresponding parents (**4** and **5**). The activities of **8** and **9** were significantly lower than that of the parent **4** in both mutations (R3X and G452X, Fig. 3B and D, respectively) tested. Introduction of the exocyclic chiral methyl group as in **10** and **11**, did not restore the readthrough activity (Fig. 3C). Furthermore, the observed decrease in comparative PTC suppression activity of **8–11** is supported by their significantly reduced inhibition of the eukaryotic protein translation (Table 1). The comparison of IC_{50}^{Euk} values reveal that **8** and **9** are 23-fold and 16.7-fold poorer inhibitors than their parent **4**, and **10** and **11** are 30-fold and 26-fold poorer inhibitors than their parent **5**.

Similar to **6** and **7**, the comparative translation inhibition tests of **8–11** in prokaryotic system (Table 1) reveals that in this system the reduction in activity is more dramatic. The observed inhibition data in prokaryotic translation, is corroborated by the significant reduction in antibacterial activity of **8–11** against both Gram-negative (*E. coli*) and Gram-positive (*B. subtilis*) bacteria, by measuring the minimal inhibitory concentration (MIC) values. Thus, the comparative biological data in Fig. 3 and Table 1 clearly show that the negative impact of the 6′-acid and 6′-amide in the pseudo-disaccharides **6** and **7** is largely retained in the subsequent pseudo-trisaccharides **8–11**.

In attempts to provide an explanation on the molecular level for the observed negative impacts of the 6′-acid and 6′-amide in the pseudo-trisaccharides **8** and **9**, in comparison with the parent compound **4**, we performed full-atom molecular dynamics (MD) followed by random acceleration molecular dynamics (RAMD)[17] simulation studies using NAMD[18] package (for details and system set-up see section S1 in ESI†). Simulations were performed for a 100 000 atom fragment of the 80S ribosome containing the decoding A site and docked compounds (Fig. S1†). The starting structures for RAMD simulations were taken from 500 ns long stable MD trajectories (Fig. S2†). For broader evaluation of the structure–activity relationship, our recently reported lead compound **2** (ref. 10) was also included. RAMD simulations were used to compare the kinetic stability of **2**, **4**, **8** and **9** by enforcing their dissociation from the A site. Total MD and RAMD simulation time was 10 μs.

Fig. 4 compares the probability of dissociation of AGs **2**, **4**, **8** and **9** from the A site, as obtained from RAMD simulations. In the 2.5 ns time frame, dissociation probability of **4** equals 99% and that of **2** is 91%, suggesting that **4** dissociates faster than **2**. This indicates that the enhanced read-through activity of **2** (as compared to that of **4**)[10] may be due to longer residence time of compound **2** in the A site. The probability of **9** is about 67%, meaning that in one-third of RAMD simulations compound **9** did not leave the A site up to 2.5 ns. This result indicates that **9** may have a higher affinity to A site than compounds **4** and **2**. Interestingly, the most stable complex in decoding A site was created by the 6′-acid **8**.

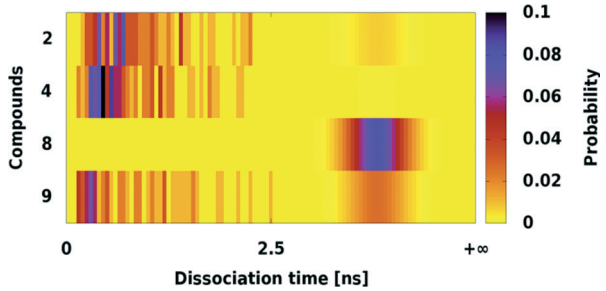

Fig. 4 Probability of dissociation of AG from the decoding A site in time from RAMD simulations. Time from 0 to 2.5 ns considers simulations in which AGs left the A site by at least 10 Å (section S1†). If compounds did not dissociate up to 2.5 ns, probabilities are depicted by Gaussian distributions spanning from 2.5 ns to infinity.

Compound **8** did not leave the A site even once under the same RAMD force (of 35 kcal mol^{-1} $Å^{-1}$) as applied for the other AGs. Actually, the dissociation of **8** has not occurred (on a 50 ns time scale) until the RAMD force was increased up to 65 kcal mol^{-1} $Å^{-1}$. The simulation data indicate that **8** and **9** have significantly enhanced stability in the A site, in comparison with **2** and **4**, even though the IC_{50}^{Euk} values of **8** and **9** are one order of magnitude higher than that of compound **4** (Table 1). In addition, since the interactions between the AGs and rRNA are mainly electrostatic,[19] it was surprising that the compound **8**-rRNA complex is so stable despite lower positive total charge of **8** (+3e) in comparison with +4e of compounds **2**, **4**, **9**. In attempts to explain the observed unique properties of the 6′-acid **8** and the 6′-amide **9**, we analyzed the short-range contacts of **2**, **4**, **8** and **9** within the A-site nucleotides as observed in simulations (Fig. 5).

All compounds have a similar interaction pattern with G1494 and U1495; ring II (N1 and N3) interacts with G1494:

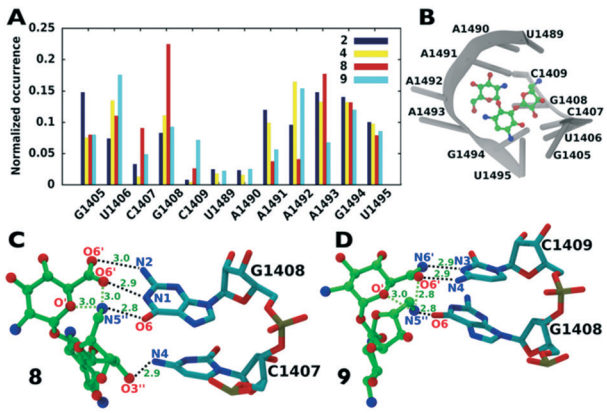

Fig. 5 (A) Occurrence of short-range interactions (within 3.2 Å) between AGs and eukaryotic A-site nucleotides derived from RAMD simulations. Normalization was carried out independently for each AG complex. (B) Positions of AGs (compound **4**) with respect to eukaryotic A site but with numbering of nucleotides as in *E. coli* ribosomes. (C and D) Examples of binding modes of compounds **8** and **9**. Inter- and intra-molecular contacts are marked as black and green dashed lines, respectively. The distances (in Å) represent averages from trajectory frames of the most occupied cluster. For clarity hydrogen atoms are not shown.

N7 and its phosphate, and with U1495:O4. These interactions anchor ring II at A site. RAMD trajectories show that compound **8** interacts with G1408 and C1407 more often than other AGs (Fig. 5A and B). The carboxyl group of **8** (O6′, ring I) is close to G1408:N1 and N2 (Fig. 5C). From three 500 ns long MD simulations, the average occurrence of hydrogen bonds of any O6′ with G1408:N1 is 57% and with G1408:N2 is about 61%. Another interaction involves **8**:N5″ (ring III) that approaches G1408:O6. Also, the ring III hydroxyl (3″-OH) hydrogen bonds with C1407:N4. Apart from interactions with G1408, another factor contributing to the stability of the **8**-rRNA complex is the intra-molecular interaction in **8** formed between ring I (O6′ and O′) and N5″ of ring III (Fig. 5C, green dashed lines). Interestingly, we also observed similar intra-molecular interaction pattern in MD simulations of free **8** in solution. Therefore, it seems that upon binding of **8** to the eukaryotic A site, its intra-molecular contacts and supposedly its conformation, are preserved.

Overall, compound **8** interacts preferentially with G1408, and this particularly strong interaction diminishes the number of contacts formed with the opposite backbone U1489–U1495 including the important A1492/93. Thus the enhanced stability of the **8**-rRNA complex is achieved by its strong interactions (especially of ring I carboxyl group) with the G1408 base and the fact that its intra-molecular bonds in solution are preserved into the A site. However, due to shifting of interactions toward the opposite backbone of helix 44, the mobility of A1492/A1493 residues, related to the efficacy of the compound **8** in translational fidelity,[9] might not be so much affected. This conclusion is supported by the data of Pilch and co-workers on the prokaryotic ribosome, demonstrating that the AG-induced reduction in the mobility of the A1492 residue in the rRNA A-site is a more important determinant of antibacterial activity than drug affinity for the A-site.[20]

Compound **9** has binding pattern that involves not only G1408 but also C1409 (Fig. 5D). The amide nitrogen of **9** (N6′) hydrogen bonds with C1409:N3, while the oxygen of the amide (O6′) interacts with C1409:N4. The carbonyl O6′ in **9** may also hydrogen bond with G1408:N1 and N2 amines but less strongly than in compound **8** (Fig. S3†). Similar as for **8**, extra stabilization of **9** in A site is achieved by its intra-molecular contacts even though these contacts are different in the A site and free compound **9** (Fig. 5D and S4†). In the A site, ring I (O6′ and O′) interacts with ring III (N5″); in solution, however, there is an interaction between N2′ (of ring I) and O″ (of ring III).

The difference between compounds **2**, **4**, **8**, and **9** lies also in their interactions with the decoding site adenines: A1491, A1492, and A1493. Both the 6′-acid **8** and the 6′-amide **9** contact A1491 less frequently than **4** and **2** (Fig. 5A and B). Compound **8** preferentially interacts with A1493 (phosphate oxygens) than with A1492. In contrast, compound **9** preferentially binds to A1492 than to A1493. Interactions of **2** and **4** with A1492 and A1493 are more balanced and they interact with both adenine phosphates.

Our MD and RAMD simulations suggest that the binding mode of the AG at the eukaryotic decoding site might influence the efficacy of AG-induced stop codon read-through. The computed binding modes of the 6′-acid **8** and the 6′-amide **9** are clearly shifted towards the nucleotide stretch G1405–C1409 of helix 44, in comparison with the binding modes of the previously reported lead structures **2** and **4**. This shift is more pronounced for the 6′-acid **8** than for the 6′-amide **9**, making the stability of **8** highest among all the AG derivatives examined. In addition, the compounds differ in their interactions with A1492 and A1493. Compounds **2** and **4** interact with both A1492 and A1493 phosphates but compound **8** prefers A1493 and compound **9** prefers A1492. Such imbalance affects the dynamics of this adenine switch, specifically its backbone, which could be critical for translational fidelity.

Conclusions

In summary, the observed structure–activity relationships of **6–11**, along with the comparative MD and RAMD simulations, indicate that the rational design of potent PTC read-through inducers is a complex process and requires consideration of not only the structure and energetics of the drug–RNA interaction but also the dynamics associated with that interaction, especially since the eukaryotic A site bulge was found more dynamically variable than the prokaryotic one.[21] This conclusion is supported by a very recently published crystal structures of the 80S ribosome in complex with paromomycin, G418, gentamicin and TC007.[22] Interestingly, AGs containing a 6′-NH_2 in ring I, including gentamicin and TC007, do not bind helix 44 at the decoding A site in a canonical fashion, rather they exhibit multiple binding sites within the large and small subunits. AGs with a 6′-OH substituent in ring I, including paromomycin and G418, however, bind helix 44 in a canonical fashion. It was suggested that the chemical composition at 6′ position of AGs and their distinct modes of interaction with 80S ribosome lead to inhibition of intersubunit movement within the eukaryotic ribosome that influence PTC read-through efficiency.

Conflicts of interest

The authors declare the following competing financial interest(s): T. B. declares that the compounds **8–11** discussed in this publication are subject to license agreement granted to a commercial third party.

Acknowledgements

This work was supported by Eloxx Pharmaceutical LTD Research Fund (Grant No. 2019230 for TB) and by the Interdisciplinary Centre for Mathematical and Computational Modelling University of Warsaw (grants G31-4 and GA65-16, for JT and TP). N. M. S. thanks to Fine Postdoctoral Fellowship at the Technion.

References

1 S. Magnet and J. S. Blanchard, *Chem. Rev.*, 2005, **105**, 477–498.
2 K. M. Keeling and D. M. Bedwell, *Curr. Pharmacogenomics*, 2005, **3**, 259–269.
3 L. V. Zingman, S. Park, T. M. Olson, A. E. Alekseev and A. Terzic, *Clin. Pharmacol. Ther.*, 2007, **81**, 99–103.
4 J. Kandasamy, D. Atia-Glikin, E. Shulman, K. Shapira, M. Shavit, V. Belakhov and T. Baasov, *J. Med. Chem.*, 2012, **55**, 10630–10643.
5 E. Shulman, V. Belakhov, G. Wei, A. Kendall, E. G. Meyron-Holtz, D. Ben-Shachar, J. Schacht and T. Baasov, *J. Biol. Chem.*, 2014, **289**, 2318–2330.
6 M. Shalev and T. Baasov, *Med. Chem. Commun.*, 2014, **5**, 1092–1105.
7 N. G. de Loubresse, I. Prokhorova, W. Holtkamp, M. V. Rodnina, G. Yusupova and M. Yusupov, *Nature*, 2014, **513**, 517–522.
8 M. Shalev, J. Kondo, D. Kopelyanskiy, C. L. C. L. Jaffe, N. Adir and T. Baasov, *Proc. Natl. Acad. Sci. U. S. A.*, 2013, **110**, 13333–13338.
9 M. Shalev, H. Rozenberg, B. Smolkin, A. Nasereddin, D. Kopelyanskiy, V. Belakhov, T. Schrepfer, J. Schacht, C. L. Jaffe, N. Adir and T. Baasov, *Nucleic Acids Res.*, 2015, **43**, 8601–8613.
10 N. M. Sabbavarapu, M. Shavit, Y. Degani, B. Smolkin, V. Belakhov and T. Baasov, *ACS Med. Chem. Lett.*, 2016, **7**, 418–423.
11 M. Manuvakhova, K. Keeling and D. M. Bedwell, *RNA*, 2000, **6**, 1044–1055.
12 P. Pfister, S. Hobbie, Q. Vicens, E. C. Böttger and E. Westhof, *ChemBioChem*, 2003, **4**, 1078–1088.
13 J. Kondo, *Angew. Chem., Int. Ed.*, 2011, **51**, 465–468.
14 P. T. Nyffeler, C.-H. Liang, K. M. Koeller and C.-H. Wong, *J. Am. Chem. Soc.*, 2002, **124**, 10773–10778.
15 L. J. van den Bos, J. D. Codee, J. C. van der Toorn, T. J. Boltje, J. H. Van Boom, H. S. Overkleeft and G. A. van der Marel, *Org. Lett.*, 2004, **6**, 2165–2168.
16 K. B. Simonsen, B. K. Ayida, D. Vourloumis, M. Takahashi, G. C. Winters, S. Barluenga, S. Qamar, S. Shandrick, Q. Zhao and T. Hermann, *ChemBioChem*, 2002, **3**, 1223–1228.
17 S. K. Lüdemann, V. Lounnas and R. C. Wade, *J. Mol. Biol.*, 2000, **303**, 797–811.
18 J. C. Phillips, R. Braun, W. Wang, J. Gumbart, E. Tajkhorshid, E. Villa, C. Chipot, R. D. Skeel, L. Kalé and K. Schulten, *J. Comput. Chem.*, 2005, **26**, 1781–1802.
19 M. Kulik, A. M. Goral, M. Jasiński, P. M. Dominiak and J. Trylska, *Biophys. J.*, 2015, **108**, 655–665.
20 M. Kaul, C. M. Barbieri and D. S. Pilch, *J. Am. Chem. Soc.*, 2006, **128**, 1261–1271.
21 J. Panecka, J. Šponer and J. Trylska, *Biochimie*, 2015, **112**, 96–110.
22 I. Prokhorova, R. B. Altman, M. Djumagulov, J. P. Shrestha, A. Urzhumtsev, A. Ferguson, C. T. Chang, M. Yusupov, S. C. Blanchard and G. Yusupova, *Proc. Natl. Acad. Sci. U. S. A.*, 2017, **114**, E10899–E10908.

